THE JOURNAL OF PHYSICAL CHEMISTRY B

Article

Cite This: J. Phys. Chem. B 2019, 123, 7372−7384

pubs.acs.org/JPCB

Ternary Complex Formation and Photoactivation of a Photoenzyme Results in Altered Protein Dynamics

Andreas Maximilian Stadler,[*,†] Judith Schneidewind,[‡] Michaela Zamponi,[§] Esther Knieps-Grünhagen,[‡] Samira Gholami,[⊥,◆] Ulrich Schwaneberg,[#,¶] Ivan Rivalta,[▽] Marco Garavelli,[⊥,○] Mehdi D. Davari,[#] Karl-Erich Jaeger,[‡,∥] and Ulrich Krauss[*,‡]

[†]Jülich Centre for Neutron Science (JCNS-1) and Institute for Complex Systems (ICS-1) and [‡]Institut für Molekulare Enzymtechnologie, Heinrich-Heine Universität Düsseldorf, Forschungszentrum Jülich GmbH, D-52425 Jülich, Germany

[§]Jülich Centre for Neutron Science (JCNS) at Heinz Maier-Leibnitz Zentrum (MLZ), Forschungszentrum Jülich GmbH, Lichtenbergstr. 1, 85748 Garching, Germany

[∥]IBG-1: Biotechnologie, Forschungszentrum Jülich GmbH, D-52425 Jülich, Germany

[⊥]Dipartimento di Chimica Industriale, Università degli Studi di Bologna, Viale del Risorgimento 4, I-40136 Bologna, Italy

[#]Institute of Biotechnology, RWTH Aachen University, Worringer Weg 3, D-52074 Aachen, Germany

[¶]DWI-Leibniz Institute for Interactive Materials, Forckenbeckstraße 50, 52056 Aachen, Germany

[▽]Université de Lyon, École Normale Supérieure de Lyon, CNRS, Université Claude Bernard Lyon 1, Laboratoire de Chimie UMR 5182, F-69342 Lyon, France

[○]École Normale Supérieure de Lyon, CNRS, Laboratoire de Chimie UMR 5182, Université de Lyon, 46 Allée d'Italie, F-69364 Lyon Cedex 07, France

Supporting Information

ABSTRACT: The interplay between protein dynamics and catalysis remains a fundamental question in enzymology. We here investigate the ns-timescale dynamics of a light-dependent NADPH:protochlorophyllide oxidoreductase (LPOR), a photoenzyme crucial for chlorophyll synthesis. LPORs catalyze the light-triggered trans addition of a hydride and a proton across the C17═C18 double bond of the chlorophyll precursor protochlorophyllide (Pchlide). Because of the lack of an LPOR structure, the global structural and dynamic consequences of LPOR/Pchlide/NADPH ternary complex formation remain elusive. Moreover, photoactivation of LPORs by low-light preillumination is controversially discussed as unequivocal proof for this phenomenon is lacking. By employing quasielastic neutron spectroscopy (QENS), we show that the formation of the ternary holoprotein complex as well as photoactivation lead to progressive rigidification of the protein. These findings are supported by thermostability measurements, which reveal different melting behavior and thermostabilities for the apo- and holoprotein ternary complexes. Molecular dynamics simulations in good agreement with the experimental QENS results suggest that the increased flexibility observed for the apoprotein stems from structural fluctuations of the NADPH and Pchlide substrate binding sites of the enzyme. On the basis of our results, in conjunction with activity and stability measurements, we provide independent proof for LPOR photoactivation, defined as a process that modifies the protein structure and dynamics, resulting in an increased substrate turnover. Our findings advance the structural and dynamic understanding of LPORs and provide a first link between protein dynamics and catalysis for this enzyme class.

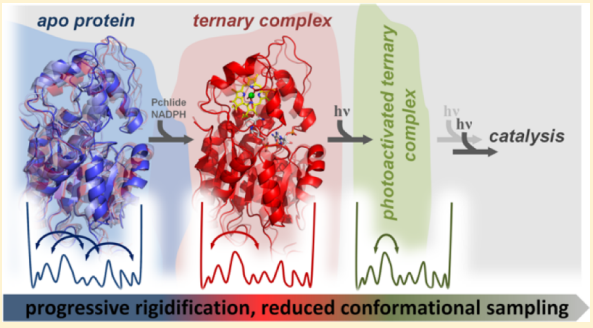

INTRODUCTION

The interplay between protein structure and dynamics is essential for the function of biological macromolecules. To enable efficient enzyme catalysis, an intricate balance between stability and flexibility is needed. Hereby, several kinds of motions, occurring on different timescales, that is, ranging from picoseconds to seconds, can directly or indirectly affect catalysis. These include local motions that impact substrate/cofactor binding[1] by acting on the active-site geometry[2] or cofactor-binding sites and[3] long-range collective motions that establish a network of coupled residues that span the entire protein[4] as well as conformational changes that are restricted to certain parts of the protein, such as lid opening and closing motions.[5] Although more and more examples that link protein

Received: July 12, 2019
Revised: August 5, 2019
Published: August 5, 2019

DOI: 10.1021/acs.jpcb.9b06608
J. Phys. Chem. B 2019, 123, 7372−7384

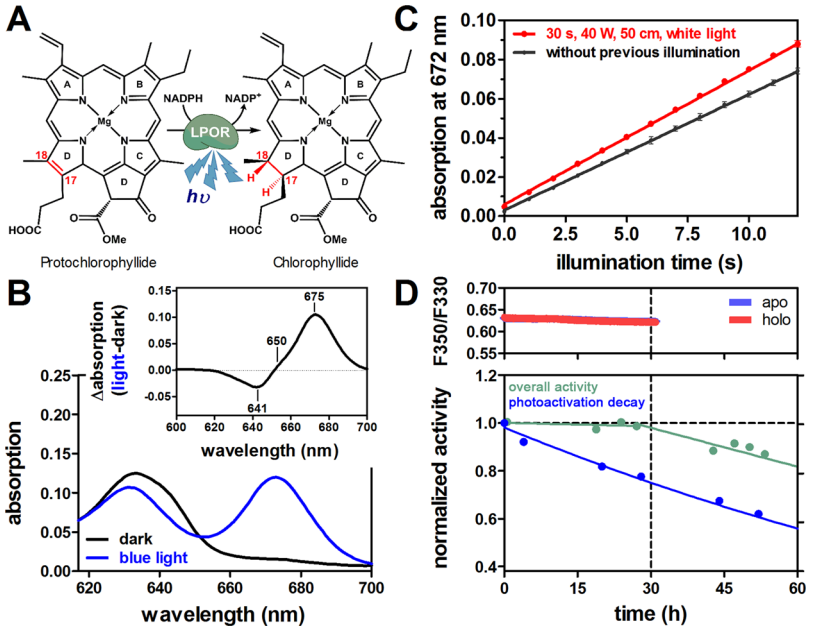

Figure 1. Activity, stability, and photoactivation of *Te*LPOR. (A) Light-dependent reduction of the C17═C18 double bond of Pchlide (highlighted in red) by LPORs yields Chlide. (B) Light-dependent activity of the *Te*LPOR holoprotein QENS sample. Absorption spectra of the "dark adapted" holoprotein before (black line) and after (blue line) blue light illumination. Spectra were matched to yield an identical absorption at 617 nm. Signature difference absorption bands[46] of the photoactive LPOR complex are highlighted in the corresponding light−dark difference spectrum (inset). (C) Light-dependent Chlide formation for "dark adapted" (black line) and photoactivated (preilluminated) (red line) holoprotein samples. Error bars correspond to the standard deviation of the mean (n = 3). (D) Stability of *Te*LPOR and decay of the photoactivated state. The stability of the *Te*LPOR apo (blue line) and holoprotein (red line) was monitored by DSF (upper panel). The stability of the ternary holoprotein complex was also assessed by monitoring light-dependent Pchlide turnover for samples incubated at 25 ± 2 °C (cyan-green filled circles, lower panel; see also Figure S2). The decay of the photoactivated state (blue filled circles, lower panel) was determined at defined times after photoactivation by activity measurements. The blue line represents the single-exponential fit of the data.

dynamics and catalysis have been provided in recent years, it is still experimentally challenging to unequivocally establish such links. Many studies in this regard have focused on dehydrogenase enzymes such as the dihydrofolate reductase[6−9] and other enzymes that catalyze proton and hydride transfer reactions. Among this class of enzymes, light-dependent NADPH:protochlorophyllide oxidoreductases (LPORs) represent one of the best studied model systems. LPORs, which are distributed throughout plants, cyanobacteria, and certain anoxygenic phototrophic microbes, catalyze the trans addition of a hydride anion and a proton across the C17═C18 double bond of the protochlorophyllide (Pchlide) D ring, resulting in the formation of chlorophyllide (Chlide)[10−13] (Figure 1A).

The LPOR/NADPH/Pchlide ternary holoprotein complex can be preformed in the dark, and catalysis is only initiated by a short pulse of light.[11−13] The latter feature has allowed detailed insight into the (ultrafast) steps associated with the light-dependent substrate turnover[14−17] and, most recently, provided the first example of a stepwise hydride transfer in a biological system.[18] In 2008, Sytina et al.[15] reported that in LPORs, for efficient catalysis, the enzyme substrate complex has to be photoactivated and that low level preillumination increases the rate of catalysis. On the basis of ultrafast pump-probe absorption difference spectroscopic data for the LPOR from *Thermosynechococcus elongatus* BP-1 (*Te*LPOR), the authors proposed a two-photon process, where the first photon turns the enzyme "on" (photoactivation) and the second photon induces catalysis.[15] Additional experiments, in which the activated sample was placed in the dark for different times, suggested that this photoactivated state is stable for at least 19 h in the dark.[15] Moreover, mid-infrared absorption difference spectroscopic data indicated that brief illumination of the enzyme substrate complex resulted in conformational changes in the secondary structure of the enzyme (i.e., evident from relatively large signals in the amide I and II regions).[15] Later on, rapid-scan Fourier-transform infrared spectroscopy at higher spectral resolution revealed the possible involvement of the Rossmann fold of LPORs and an increased solvent exposure of the protein after photoactivation.[19] More recently, the proposed photoactivation process has been linked to the formation of Pchlide−Chlide dimers in the protein, and the two-photon process has been called into question.[20] The nature of the photoactivation-induced conformational change, which irrespective of its role in catalysis has been proven to exist, has not been further investigated, and the photoactivation process itself remains controversially discussed. Likewise, the conformational transitions that occur due to the formation of the LPOR/NADPH/Pchlide ternary holoprotein complex remain structurally largely elusive, which is due to the fact that at present, no crystal structure is available for the LPOR system.[12,21]

Given the similarity between dihydrofolate reductases (DHFRs) and LPORs, which possess a similar catalytic mechanism, it is tempting to speculate that for LPORs, like in DHFR, protein motions and conformational dynamics also play an important role.[22] To the best of our knowledge, the interplay between internal protein dynamics, the formation of the LPOR/NADPH/Pchlide ternary holoprotein complex, and the aforementioned photoactivation process, have not been investigated. To address this issue, quasielastic neutron spectroscopy (QENS) experiments have been performed. The technique is well-suited to measure the localized dynamics

DOI: 10.1021/acs.jpcb.9b06608
J. Phys. Chem. B 2019, 123, 7372−7384

of biological macromolecules on the picosecond to nanosecond time scale and on the Ångstrom length scale.[23] QENS is predominantly sensitive to the motions of protons because of the large incoherent scattering cross-section of ^{1}H compared to all other chemical elements occurring in biological macromolecules including ^{2}H. Average protein dynamics are probed by QENS as hydrogen atoms are distributed homogeneously in proteins.

In the present contribution, we investigate the dynamics of the NADPH/Pchlide-free LPOR apoprotein, the LPOR/NADPH/Pchlide ternary holoprotein complex, and the ternary complex, after photoactivation by QENS. Our study provides strong evidence that the formation of the ternary holoprotein complex as well as photoactivation result in progressive rigidification of the protein. Thermostability measurements and molecular dynamics (MD) simulations corroborate this finding, while the latter suggests that the flexibility observed for the apoprotein stems from structural fluctuations of the NADPH and Pchlide substrate binding sites of *Te*LPOR, with the rigidification of the dark-adapted and the photoactivated holoprotein therefore likely occurring at those sites. Based on this data, in conjunction with activity measurements, spectroscopic characterization, and stability analyses, we hereby redefine photoactivation as the structural/dynamic process that is triggered by limited Pchlide turnover (and likely the presence of Pchlide−Chlide dimers in the protein) due to low-light steady-state preillumination.

METHODS

Strains and Plasmids. For cloning purposes, *Escherichia coli* DH5α was used. Heterologous expression was carried out using *E. coli* BL21(DE3). The gene encoding for the LPOR from *T. elongatus* BP-1 (*Te*LPOR, UniProt ID: Q8DLC1) was synthesized without codon optimization by ThermoFisher Scientific/Life technologies (Waltham, MA, USA). A 5′-*Nde*I and a 3′-*Sal*I restriction endonuclease recognition site was added to the synthetic gene to facilitate subcloning into pET28a (Merck/Novagen, Darmstadt, Germany) as the expression vector. This resulted in the plasmid pET28a-*Te*LPOR, which in addition to the *Te*LPOR encoding gene contained an in-frame fused N-terminal 20 amino acid long His_6-tag (tag sequence: MGSSHHHHHHSSGLVPRGSH) that facilitated the purification of the protein by immobilized metal ion affinity chromatography (IMAC). The final construct was verified by sequencing (SeqLab, Göttingen, Germany).

Heterologous Gene Expression and Protein Purification. For heterologous expression of the *Te*LPOR encoding gene, *E. coli* BL21(DE3) cells were transformed with the plasmid pET28a-*Te*LPOR. Expression cultures were grown in 5 L nonbaffled Erlenmeyer flasks using 500 mL of auto-induction medium (modified according to Studier et al.[24]) supplemented with 50 μg/mL kanamycin to facilitate plasmid maintenance. In brief, the medium consisted of 445 mL of Terrific-broth medium (Carl-Roth GmbH) supplemented with 4 mL/L glycerol, 5 mL of 50 g/L glucose, and 45 mL of 20 g/L lactose. Cultures were initially grown for 2 h at 37 °C under constant agitation (250 rpm). Subsequently, the temperature was reduced to 15 °C, and the cultures were grown for additional 48 h. After harvesting by centrifugation (30 min, 6750*g*, 4 °C), the cells were resuspended in a suitable volume of 20 mM Tris/HCl, 500 mM NaCl, 20% (w/v) glycerol, pH 7.5. Cell disruption was achieved by passing the corresponding cell suspensions (10% (w/v) wet cells) five times through a EmulsiFlex-C5 high-pressure homogenizer (AVESTIN, Ottawa, Canada) (1000 bar pressure). The recombinant *Te*LPOR protein was purified by IMAC as previously described for *Ds*LPOR.[10] IMAC-purified protein samples were desalted by gel filtration using a Sephadex G25 column [560 mL column volume (CV), XK50/30, GE Healthcare Life Science, VWR International GmbH, Langenfeld Germany]. As the final buffer, 20 mM Tris/HCl pH 8.5 supplemented with 100 mM NaCl was used. For the envisioned neutron scattering experiments, it is advantageous that the samples contain as less salts and additives, that is, containing additional protons, as possible. Usually, *Te*LPOR and other LPORs are purified using high-salt buffers (500 mM NaCl) containing 20% glycerol.[10,25,26] This significantly improves the solubility of the protein. To minimize buffer effects, we therefore employed here a buffer containing only 100 mM NaCl without glycerol. Consequently, the protein concentration of the sample was kept low (<10 mg/mL) during all steps of the preparation procedure to avoid precipitation of the protein. Desalted protein samples were frozen at −80 °C and lyophilized using a Lyovac GT2 (Steris GmbH, Hürth, Germany) freeze dryer.

Pchlide Production and Purification. For the production of the commercially not available *Te*LPOR Pchlide substrate, *Rhodobacter capsulatus* ZY5[27] was used. The strain was grown in nonbaffled Erlenmeyer flasks in the dark at 30 °C under constant agitation (130 rpm) by using VN-Medium (10 g/L yeast extract, 5.7 μM K_2HPO_4, 2 μM $MgSO_4$, pH 7.0). Cultures were inoculated to an optical density $(OD)_{660nm}$ of 0.01 and grown under microaerobic conditions (culture volume 50% of the flask volume). To remove the secreted Pchlide from the culture medium, hydrophobic polyurethane cubes (edge length 1 cm) were added during cultivation. After 24 h, the cubes were removed from the cultures and washed with tricine buffer (10 mM tricine pH 7.5) to remove cells attached to the cubes. Pchlide was extracted with 100% methanol, and the extract was filtrated (cellulose acetate filter membranes, pore size 0.45 μm). Pchlide purification was achieved by column chromatography using an ÄKTAbasic FPLC system (GE Healthcare, Solingen, Germany). The filtrated methanolic extract was diluted with tricine buffer to a final concentration of 40% (v/v) methanol and loaded onto a TAC15/500LGO-SR-2 column (YMC ECO^{PLUS}, YMC Europe GmbH, Dinslaken, Germany) filled with C-18 solid-phase extraction material (Sep-Pak, Waters, Milford, MA, USA). Before loading, the column was equilibrated with a 40:60 methanol/tricine buffer mixture. After two CVs, the methanol concentration was increased to 50% and after additional 25 CVs, it was further increased to 60%. To facilitate the Pchlide elution, the methanol/tricine buffer ratio was adjusted to 75:25. The final Pchlide eluate was diluted with tricine buffer to a final methanol concentration of 25%. Subsequently, Pchlide was extracted by liquid−liquid extraction with fresh diethyl ether. The resulting ether extract was dried by adding $MgSO_4$, and the ether was evaporated using a rotary evaporator (Rotavapor R-100, Büchi, Flawil, Switzerland). The dried Pchlide powder was stored at −20 °C in the dark under an argon atmosphere. For the reconstitution of the *Te*LPOR ternary complex, dried Pchlide was resuspended in methanol-d_4 (CD_3OD, 99.8% atom D) (Sigma, St. Louis, MI, USA).

QENS Sample Preparation. For the preparation of the *Te*LPOR apo-protein sample, the purified, lyophilized protein

DOI: 10.1021/acs.jpcb.9b06608
J. Phys. Chem. B 2019, 123, 7372−7384

was dissolved in the initial volume D_2O (99.9% atom D) (Sigma, St. Louis, MI, USA). To achieve complete substitution of all exchangeable protons for deuterium, the sample was again lyophilized, and the procedure was repeated once. To produce the *Te*LPOR/NADPH/Pchlide ternary holoprotein complex, the purified, lyophilized *Te*LPOR sample was dissolved in the initial volume of D_2O. Subsequently, the sample was again lyophilized, dissolved in the initial volume of D_2O, and diluted with D_2O to a final protein concentration of 0.75 mg/mL (19.8 μM). Incubation times in D_2O were identical for all samples. Initially, tests were performed to validate sample integrity (in terms of activity) after multiple lyophilization/D_2O reconstitution cycles, which did not reveal any significant loss of activity during two consecutive lyophilization cycles. Finally, the diluted *Te*LPOR/NADPH/Pchlide ternary holoprotein complex was reconstituted by mixing 19.7 μM NADPH (as powder) and 19.8 μM purified Pchlide (in CD_3OD) with the diluted *Te*LPOR sample [7% (v/v) CD_3OD concentration in the sample]. Subsequently, the lyophilized samples of the reconstituted complex as well as of the corresponding pigment-free apoprotein were placed in flat aluminum sample holders (0.3 mm internal thickness, 30 mm width, and 40 mm height) and dried in a desiccator over silica gel until no further loss of weight was observed. The dried protein powders were rehydrated to a level of 1.6 g D_2O/1 g protein in a saturated D_2O atmosphere. This corresponds to about 4-fold hydration envelope. Highly viscous, yet optically clear, protein samples were obtained, which did not show visual evidence for protein or Pchlide precipitation. For each experiment, (apoprotein, holoprotein, and photoactivated holoprotein) separate samples, each containing about 100 mg of *Te*LPOR protein, were prepared. Furthermore, 160 mg of D_2O buffer was measured as the background, which contains as much D_2O as in the hydrated protein samples. All final samples were tested for functionality.

LPOR Activity and Stability Measurements. Light-dependent Pchlide turnover was measured spectrophotometrically by monitoring the light-dependent production of the Chlide reaction product, as described previously.[10] Reactions were performed in a reaction buffer [20 mM Tris pH 7.5 buffer supplemented with 500 mM NaCl and 20% (w/v) glycerol]. Additives (70 μM DTT, 0.03% (v/v) Triton X-100) were added separately to the reaction. Reproducible illumination was achieved by using a blue-light emitting light-emitting diode (LED) (450 nm; 2.6 mW cm^{-2}) mounted on top of the cuvette. Pulsed illumination was enabled by employing a microcontroller-controlled LED driver, Arduino UNO (Smart Projects, Italy).[10] Data was analyzed using a home-written shell script, which filters and removes spectra that contain illumination events. Pchlide and Chlide were quantified photometrically using previously reported molar extinction coefficients (Pchilde: ε_{630nm} = 23 950 M^{-1} cm^{-1}; Chlide: ε_{670nm} = 69 950 M^{-1} cm^{-1}).[26] Long-term stability of the ternary holoprotein complex was assessed by monitoring light-dependent Pchlide turnover for samples incubated at 25 ± 2 °C for up to 60 h. LPOR activity, determined at defined times during incubation, was measured as described above and was expressed relative to the activity at time t = 0.

Photoactivation Measurements. Samples of the *Te*LPOR/NADPH/Pchlide ternary holoprotein complex were prepared in the dark (see section LPOR Activity and Stability Measurements). Samples were split, and one half was preilluminated for 30 s using a 40 W tungsten lamp placed at a distance of 50 cm from the sample (illumination conditions reported by Sytina et al.[15]). Subsequently, LPOR activity was determined for the "dark-adapted" and the preilluminated samples by following the increase in absorption of the Chlide reaction product at 672 nm. The decay of the photoactivated state, populated after preillumination of the holoprotein complex, was followed by illuminating a preilluminated sample (prepared as described above) at defined time points after preillumination and incubation in the dark. To determine the activity, at each time point, the samples were illuminated with blue light for 6 s, and the amount of the formed Chlide reaction product was quantified. The amount of the formed Chlide reaction product is expressed relative to the amount formed at t = 0.

DSF for Thermal-Unfolding/Stability Analyses. For differential scanning fluorimetry (DSF) measurements, a Prometheus NT.Flex (NanoTemper Technologies GmbH, Munich, Germany) instrument was used, which precisely measures thermal-unfolding-induced changes in tryptophan fluorescence. *Te*LPOR apo- and reconstituted holoprotein samples (10 μL) with a concentration of 0.65 mg/mL were subjected to a linear unfolding ramp (0.5 °C/min, from 15 to 90 °C). The intrinsic protein fluorescence was monitored continuously (18 data points per min) at 350 and 330 nm. Unfolding transition midpoints were determined from the first derivative of the fluorescence ratio (F_{350}/F_{330}) by using the Quick Peaks gadget implemented in Origin 9.0G (OriginLab Corporation, Northampton, MA, USA). Identically prepared samples were used for thermal stability measurements, which were conducted at a fixed temperature of 25 °C. DSF was measured over a period of 30 h.

Neutron Scattering Experiments. Neutron scattering was measured on the high-resolution backscattering instrument SPHERES operated by JCNS[28,29] at the Heinz Maier-Leibnitz Zentrum (MLZ), Garching, Germany. The incident neutron wavelength was 6.27 Å. SPHERES has an energy resolution of approximately 0.66 μeV full width at half-maximum (fwhm) at large scattering angles. Spectra were recorded over an energy-transfer range of −30 to +30 μeV. QENS data were analyzed for a scattering vector range between 0.34 and 1.76 $Å^{-1}$. Energy channels were binned for better statistics. Measured intensities were normalized to vanadium and transformed into energy transfer and scattering vector space. All samples were mounted in Al-flat cells and were oriented at 135° with respect to the incident beam. Resolution functions were measured with a 1 mm-thick vanadium slab. Scattered intensities of the empty cell including buffer were subtracted from the measured protein solutions. All measurements were performed at 298.2 K.

On SPHERES, the samples of apo-*Te*LPOR, holo-*Te*LPOR in the dark and the buffer have been measured for 24 h. The sample holder containing holo-*Te*LPOR was taken out of the cryostat, opened, and illuminated with a 40 W tungsten lamp at a distance of 50 cm for 5 min. The sample holder was then sealed again with an indium wire. The illuminated holo-*Te*LPOR was reinserted into the cryostat, and the QENS experiment was restarted. Neutron scattering data of illuminated holo-*Te*LPOR were accumulated over a period of 12 h to obtain sufficient statistics.

QENS Data Analysis. A simplified model for QENS spectra of internal protein dynamics is given by[23,30]

DOI: 10.1021/acs.jpcb.9b06608
J. Phys. Chem. B 2019, 123, 7372−7384

Table 1. Dynamic Parameters Determined from QENS

sample	D_{eff} (Å^2/ns)	$\sqrt{\langle u^2 \rangle}$ (Å)[a]	RMSD(τ) (Å)[b]	D_{int} (Å^2/ns)	τ (ps)
apo-LPOR	0.081 ± 0.003	2.26 ± 0.05	2.12 ± 0.05	13.2 ± 0.8	130.7 ± 3.7
holo-LPOR (dark-adapted)	0.196 ± 0.003	1.93 ± 0.03	1.62 ± 0.19	48.3 ± 2.4	85.0 ± 1.3
holo-LPOR (photoactivated)	0.141 ± 0.004	1.75 ± 0.03	n.a.	33.9 ± 2.0	86.1 ± 2.2

[a]MSD ($\langle u^2 \rangle$) expressed as $\sqrt{\langle u^2 \rangle}$ to allow direct comparison to published data (see below). [b]Determined from MD simulations as the mean and standard deviation of the mean from three independent apo- and holoprotein trajectories. n.a. not applicable.

$$S_I(q, \omega) = A_0(q) \times \delta(\omega) + [1 - A_0(q)] \times L(q, \omega) \quad (1)$$

where $A_0(q)$ is the elastic incoherent structure factor (EISF). The quasi-elastic broadening due to localized diffusive internal protein motions is approximated by 1 effective Lorentzian $L(q,\omega)$. In solution, proteins additionally show centre-of-mass and rotational diffusion. The total scattering function $S_{total}(q,\omega)$ for motions visible by QENS is then the convolution of the dynamic structure factors of global diffusion $S_G(q,\omega)$ and of internal dynamics $S_I(q,\omega)$. It was shown that in the q-range probed by QENS, rotational and translational diffusions of the protein can be described by 1 effective Lorentzian.[31−33] Therefore, the total dynamic structure factor then reads as

$$S_{total}(q, \omega) = A_0(q) \times L_G(q, \omega) + [1 - A_0(q)] \times L_{G+I}(q, \omega) \quad (2)$$

with the 2 Lorentzians

$$L_G(q, \omega) = \frac{1}{\pi} \cdot \frac{\Gamma_G(q)}{(\hbar\omega)^2 + \Gamma_G(q)^2} \quad (3)$$

and

$$L_{G+I}(q, \omega) = \frac{1}{\pi} \cdot \frac{\Gamma_G(q) + \Gamma_I(q)}{(\hbar\omega)^2 + [\Gamma_G(q) + \Gamma_I(q)]^2} \quad (4)$$

where $\Gamma_G(q)$ and $\Gamma_G(q) + \Gamma_I(q)$ are the half-widths at half-maximum (hwhm) of the Lorentzians accounting for global and internal diffusive motions, respectively. The total theoretical scattering function plus linear background was convoluted with the instrumental resolution function and fitted to the measured spectra.

MD Simulations. The initial coordinates for apo- and holo-*Te*LPOR enzyme of *T. elongatus* were constructed from the refined homology model (with catalytically competent active site geometry) described by Gholami et al.[21] Two sets of independent MD simulations for apo- and holo-*Te*LPOR [with the bound Pchlide (PCL) substrate and the cofactor NADPH] were carried out. The PROPKA 3.1 program[34] was used to assign the protonation states of titratable residues on the basis of pK_a values and visual inspection. Atomic charges and force field parameters for PCL and NADPH were adapted from a previous work.[21] Hydrogen atoms were added by using the tleap module in Amber 12,[35] and the Amber ff10 force field[36,37] for the protein was employed. The apo- and holo-*Te*LPOR enzyme were solvated in a 20 Å rectangular box of TIP3P water molecules[38] and neutralized by adding counter-ions. The resulting simulation setup consisted of 35 448 water molecules and overall 111 894 atoms for holo and 35 450 water molecules and overall 111 755 atoms for the apo enzyme. Initially, the solvent and the ions were minimized followed by the whole system minimization using 10 000 steps of steepest descent followed by 3000 steps of conjugate-gradient minimization. Afterward, the system was heated slowly from 0 to 300 K for 50 ps. In MD simulations, constant pressure periodic boundary conditions using the particle mesh Ewald[39] method were employed. Electrostatic and van der Waals interactions were calculated using a cutoff of 10 Å. After the heating step, the systems were equilibrated for 1000 ps at 300 K. Three independent production runs each for 20 ns were carried out for apo- and holo-*Te*LPOR. Isotropic position scaling and the Berendsen thermostat[40] method were used to keep the system at 1 atm and 300 K, respectively. Further details of the methodology is reported in ref 21. All classical MD simulations were performed using the Amber 12 program.[35] The obtained MD simulation trajectories were analyzed and visualized with AmberTools 14[41] and Pymol.[42] Root-mean-square deviation (RMSD) and root-mean-square fluctuation (RMSF) values were calculated for each trajectory after aligning to the minimized structure. RMSF values were calculated using 1 ns windows for all nonexchangeable hydrogen atoms of the enzyme for all MD trajectories after convergence of RMSD. RMSD(τ), as a proxy for the QENS-derived mean square displacement (MSD; $\sqrt{\langle u^2 \rangle}$; see Table 1) was calculated from the per-residue RMSF at a time resolution of 1 ns as the average over all per-residue values.[43] The MMTSB toolset (ref 44) was used to perform cluster analysis on the *Te*LPOR active site with *K*-means clustering algorithm, employing a 2 Å RMSD as cutoff radius.

RESULTS

***Apo* LPOR Can Be Reconstituted with NADPH and Pchlide To Yield the Photoactive LPOR Ternary Holoprotein Complex.** As a model system for our study, we selected the cyanobacterial LPOR of *T. elongatus* BP-1 (*Te*LPOR), which can readily be produced in large quantities, is highly stable,[45] and represents the best characterized LPOR in terms of photophysics and reaction mechanism.[15,17,18,20,25,31] Samples of the *Te*LPOR apoprotein and the reconstituted NADPH/Pchlide/*Te*LPOR ternary holoprotein complex were prepared as described in the Methods section. To test whether the *Te*LPOR holoprotein sample, prepared for QENS experiments is photoactive, we performed an illumination experiment. Samples of the "dark adapted" holoprotein were illuminated for 6 s with blue light. Absorption spectra were recorded before and after illumination (Figure 1B). After illumination, the built up of an absorption band with a maximum at around 672 nm is observed, which represents the Chlide reaction product.[46−48] Moreover, the light−dark absorption difference spectrum shows a negative band at around 641 nm, a weak shoulder at 650 nm, and a positive band at around 675 nm (Figure 1B; inset), which is a spectral signature of the photoactive LPOR complex as reported for gel-filtration purified *n*-dodecyl-β-D-maltoside solubilized prolamellar bodies obtained from etiolated wheat

DOI: 10.1021/acs.jpcb.9b06608
J. Phys. Chem. B 2019, 123, 7372−7384

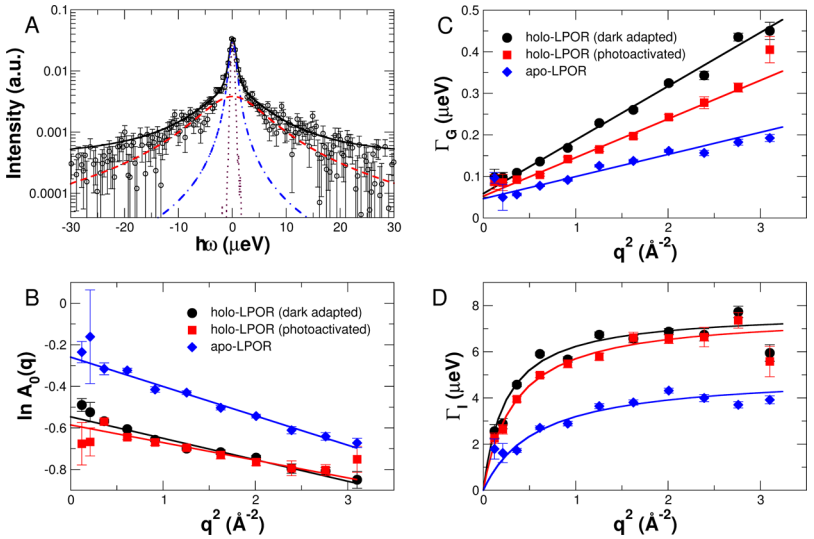

Figure 2. QENS studies of *Te*LPOR. (A) Measured QENS spectrum at the scattering vector of q = 1.76 Å^{-1} of *Te*LPOR apoprotein. Symbols represent experimental data. The total fit according to eq 2 is given by the black solid line. The components of the fit are the narrow (blue dashed-dotted) and broad (red dashed) Lorentzians representing global protein diffusion and the convolution of global and internal protein dynamics. The instrumental resolution function is given by the brown dotted line. All fit functions are convoluted with the instrumental resolution function. Only every second data point is shown for clarity. (B) EISF of apo-LPOR, dark-adapted holoprotein, and the photoactivated holoprotein. Solid lines are linear fits to the data to extract the MSDs. (C) Line-widths of the narrow Lorentzian that describe global protein diffusion. Solid lines are linear fits to extract the global protein diffusion coefficients. (D) Line-widths describing internal diffusive protein dynamics. Solid lines are fits using a jump-diffusion model.

leaves.[46] Similar signatures were also detected for recombinant barley LPOR B (studied as a fusion protein with the maltose-binding protein).[49]

Low-Level Steady-State Preillumination Results in Minimal Pchlide Turnover, Which Is Accompanied by Photoactivation. We next reproduced the experiment by Sytina et al.[15] and tested whether brief low-level preillumination, which does not result in significant Pchlide turnover (Figure S1), results in higher LPOR activity compared to a sample which was not preilluminated. The preillumination conditions employed here were identical to the steady-state experiment described by Sytina et al.,[15] yielding minor amounts of the Chlide reaction product (Figure S1 blue line). Figure 1C clearly demonstrates that the preilluminated samples show indeed increased activity compared to the not preilluminated ones, yielding initial rate velocities of 0.87 ± 0.04 U/mg (preilluminated) and 0.78 ± 0.01 U/mg (not preilluminated). This corresponds to an 11% increase in activity due to preillumination. Last, we monitored the decay of the photoactivated state as well as the stability of apo- and holoprotein samples over extended periods of time (Figure 1D), that is, to verify protein stability during the long measuring times needed for our QENS experiments.

Sytina et al. suggested that the photoactivated state is stable at room temperature for at least 19 h.[15] To assess the decay of the photoactivated state, we preilluminated a sample containing *Te*LPOR, Pchlide, and NADPH in assay buffer, using the illumination setup as described above. The preilluminated sample was subsequently aliquoted and kept at 25 ± 2 °C in the dark for extended periods of time. At defined time intervals, aliquots were illuminated for 6 s, and the amount of the formed Chlide product was estimated from the corresponding ultraviolet−visible (UV−vis) spectra. Over time, the amount of formed Chlide decreased as depicted in Figure 1D (blue filled circles; decay of photoactivated state). From a single-exponential fit of the data, the lifetime of the photoactivated state can be estimated to $\tau_{act} \approx 130$ h. The full dataset for two independent measurements on two independent protein preparations is shown in Figure S2. The reported τ_{act} value, however, represents only a rough estimate as we could not measure long enough (>100 h) to ensure complete decay of the photoactivated state because of loss of sample integrity at very long incubation times. To rule out that this apparent decrease in activity is due to inactivation of the enzyme, we performed nano-DSF-based thermostability experiments, in which the intrinsic protein fluorescence (aromatic amino acids) is monitored continuously during incubation at 25 °C (Figure 1D; upper panel; F_{350}/F_{330}). During 30 h of measuring time, that is the maximum measuring time used in our below presented QENS measurements, neither the *Te*LPOR apo- nor the *Te*LPOR holoprotein samples did show any significant unfolding. Additionally, we also measured the light-dependent activity of a *Te*LPOR sample incubated for at least 60 h at 25 ± 2 °C (Figure 1D, red filled circles; normalized activity). During the first 30 h, we did not observe any significant loss of activity, whereas at later time points, *Te*LPOR appears to lose about 10−15% of its activity. Please note that *Te*LPOR is a thermophilic protein possessing a melting temperature of around 70 °C (see Figure S3).

Ternary Complex Formation and Photoactivation Results in Altered LPOR Protein Dynamics. After validating the stability and functionality of the prepared *Te*LPOR apo- and holoprotein samples, we adapted the illumination conditions established by Sytina et al.[15] for a diluted protein sample to the rehydrated, highly viscous, optically dense protein samples prepared for QENS experiments. Here, illumination of the rehydrated sample for 5 min yielded identical Pchlide turnover as compared to 30 s illumination of the dilute solution (Figure S1). Using these conditions, we investigated the dynamics of the *Te*LPOR apoprotein, the dark-adapted holoprotein, and the illuminated/photoactivated holoprotein. QENS of *Te*LPOR apo- and dark-

DOI: 10.1021/acs.jpcb.9b06608
J. Phys. Chem. B 2019, 123, 7372−7384

adapted holoprotein was measured for 24 h. After illumination of the holoprotein sample (see experimental procedures for details), QENS was measured for only 12 h to rule out any significant recovery of the photoactivated state during the measurement while still providing sufficient statistics. Assuming single-exponential decay of the photoactivated state, occurring with a lifetime of $\tau_{act} \approx 130$ h, about 10% of the molecules should recover within 12 h of measuring time. A typical QENS spectrum of the *Te*LPOR apoprotein at the largest scattering vector $q = 1.76$ Å^{-1} is shown in Figure 2A.

The extracted hwhm from the quasi-elastic broadening is shown in Figure 2C,D for illustrative conditions. The measured Γ_G and Γ_I report on global protein diffusion and internal localized dynamics, respectively.

Effective diffusion coefficients that account for global protein diffusion (rotational and translational diffusion) were calculated according to $\Gamma_G(q) = D_{eff} \cdot q^2$. The D_{eff} values determined in that approach are between 1.2 and 1.3 larger than the theoretical value of pure translational diffusion due to the contribution of rotational diffusion that increases the linewidths of the measured QENS spectra.[31,50,51] The exact value depends on the anisotropic shape of the protein and hydration. The observed values of Γ_G are close or below the energy resolution of the spectrometer, which is at around 0.66 μeV (fwhm) at large scattering angles. However, the Γ_G follow the expected linear behavior indicative of global protein diffusion when plotted versus q^2, see Figure 2C. The non-zero intercept of $\Gamma_G(q \to 0)$ with around 0.05 μeV might be indicative of a small contribution of multiple scattering that is also observed in the EISF (see below). An eventual and more interesting interpretation might be to associate that intersect to a q-independent rate that could be attributed to a slow internal process in the protein with a relaxation rate of $\tau = \frac{\hbar}{0.05\ \mu eV} = 13$ ns, which is well in the typical range of large-scale protein domain motions that have been observed by high-resolution neutron spectroscopy before.[52,53] However, as that dynamic process is far below the energy resolution of the SPHERES neutron spectrometer, we cannot make any strong statements about the effect of multiple scattering or the observation of another internal dynamic process here. Obtained values of D_{eff} are given in Table 1. As highly concentrated and viscous protein samples have been measured, the observed values of D_{eff} ranging between 0.1 and 0.2 Å^2/ns are strongly reduced as compared to the value of translational diffusion of *Te*LPOR of 7.4 (apo) and 7.5 Å^2/ns (holo) at infinite dilution. However, the fact that global protein diffusion is observed under all conditions demonstrates that the proteins are sufficiently hydrated above one hydration layer. Hence, internal protein dynamics are not suppressed due to the lack of hydration water. The larger D_{eff} value of apo-*Te*LPOR indicates a lower concentration of the apoprotein as compared to the holoprotein. During illumination of holo-*Te*LPOR, a small amount of D_2O apparently evaporated, which results in a reduction of the obtained D_{eff} value of the illuminated holoprotein as compared to the dark-adapted state. The directly scattered neutron intensity from light-illuminated LPOR was less than that of dark-adapted LPOR, which supports our hypothesis on water evaporation.

Quantitative information on internal protein dynamics can be extracted from the obtained Γ_I-values. The dependence of Γ_I as a function of q^2 indicates the presence of diffusive internal motions in the protein that can be interpreted with a simple analytical model function describing jump-diffusive motions according to $\Gamma_I = \frac{D_{int} \cdot q^2}{1 + D_{int} \cdot q^2 \cdot \tau}$, with the effective diffusion coefficient of internal dynamics D_{int} and the residence time τ between jumps. Obtained values of D_{int} and τ are given in Table 1. At large length-scales, probed in the small q^2-range, diffusive motions of H atoms attached to amino acids or to the protein backbone are visible, and Γ_I follows the $\Gamma_I = D_{int} \cdot q^2$ dependence with the average diffusion coefficient D_{int}. Deviation of the first data point apo-LPOR from that behavior might be due to confinement effects that would be visible at even smaller q-vectors. At local distances being visible at larger q^2-values, the granularity of motions in the protein becomes visible. Localized jumps of amino acids or the backbone chain between slightly different structural orientations result in the plateau, which is visible at high q^2-values (Figure 2D). This data provides information about the energetic landscape and the rates of transitions between conformational substates[54] of a given conformational state (here apoprotein, holoprotein, and photoactivated holoprotein; see Discussion section for details). Diffusive motions would hereby correspond to motions within the conformational substate. After a certain time, the protein moves to a slightly different conformational substate. The average time that the H atoms are sitting in one conformational substate is reflected by the residence time τ, which causes the plateau of the $\Gamma_I = 1/\tau$ in the high q^2-limit. With regard to these characteristics, we observe a slower internal diffusion coefficient and a larger residence time τ for the apoprotein, as compared to the ternary holoprotein complex. In contrast, photoactivation results in a reduced internal diffusion coefficient, whereas residence times remain on a comparative level as determined for the "dark-adapted" holoprotein.

Information on the amplitude of internal protein dynamics is contained in the experimentally determined EISF abbreviated as $A_0(q)$. The values of $A_0(q)$ are shown in Figure 2B. MSDs $\langle u^2 \rangle$, as a measure for the flexibility and the conformational space that is accessible to the protein, were calculated from the EISF according to[55,56]

$$\langle u \rangle^2 = \frac{-6A \cdot \ln A_0(q)}{q^2}$$

where A is a prefactor to account for the non-zero intercept of the data for $q^2 \to 0$. Here, again the non-zero intercept might be attributed either to (i) multiple scattering or (ii) the presence of a slow dynamic process with a large amplitude. Deviation of the first two data points of dark-adapted holo-LPOR from linear behavior as compared to apo-LPOR might agree with point (ii) and correspond to a large-scale domain motion with a MSD larger than 1 nm. However, neutron backscattering is not sensitive to probe dynamics occurring in the timescale of some 10 ns with amplitudes of motions of several nanometers, and we limit our discussion in the following on the MSDs that could be obtained from the EISF data using linear regression. The obtained values of $\langle u^2 \rangle$ are reported in Table 1, with larger values suggesting increased flexibility of the protein. The data thus suggests that formation of the holoprotein ternary complex and photoactivation results in progressive rigidification of the protein, as evidenced by the decrease in $\langle u^2 \rangle$ in the order apoprotein $\gg$ holoprotein > photoactivated holoprotein.

DOI: 10.1021/acs.jpcb.9b06608
J. Phys. Chem. B 2019, 123, 7372−7384

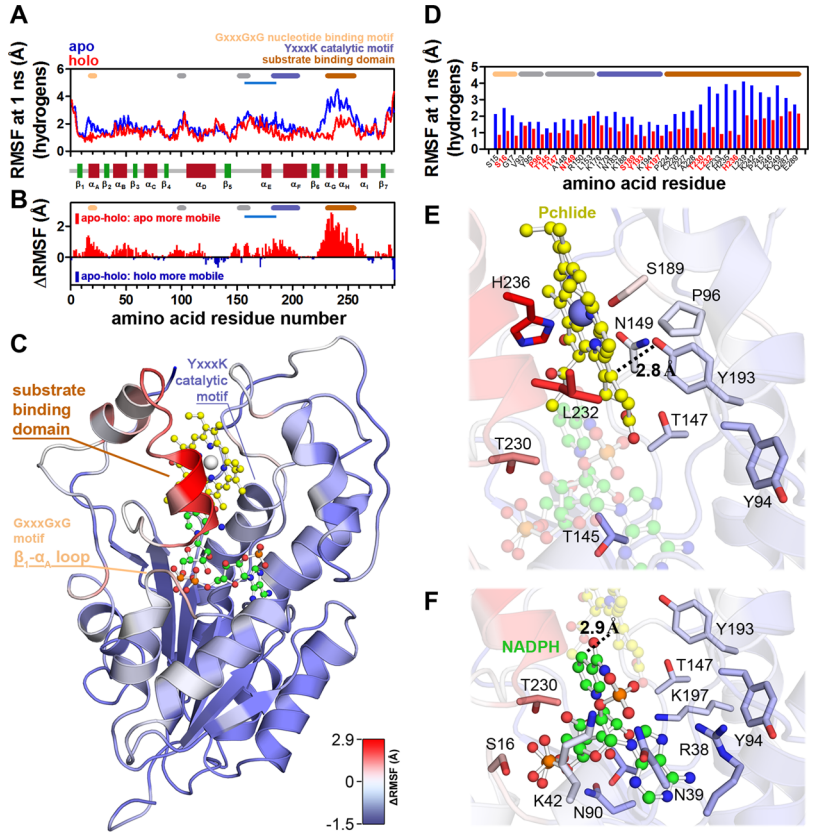

Figure 3. MD simulations of the *Te*LPOR apoprotein and the ternary holoprotein complex. (A) Mean RMSF per residue obtained from three independent simulations of apo (blue) and holo (red) *Te*LPOR. (B) Apo−holo ΔRMSF per residue, highlighting residues with increased (positive values; red) and decreased flexibility (negative values; blue) relative to the apoprotein. (C) Structure of the *Te*LPOR ternary holoprotein complex in cartoon representation (colored according to ΔRMSF), with NADPH and Pchlide shown as balls and sticks with green and yellow carbon atoms, respectively. Nitrogen, oxygen, and phosphorous atoms are shown in blue, red, and orange. (D) Apo- (blue bars) and holoprotein (red bars) RMSF values for selected active site residues. Functionally important regions such as the NADPH-binding motif (light orange), the YxxxK catalytic motif (dark blue), the Pchlide substrate binding domain (dark orange), the extended LPOR extra loop (light blue), and other regions harboring functionally relevant residues (in grey) are marked in A-D. Pchlide (E) and NADPH (F) binding site of *Te*LPOR. Selected residues, constituting the active site or mediating Pchlide and NADPH binding, are shown in stick representation, with carbon atoms colored according to ΔRMSF. Interatomic distances for the active site Tyr193-OH···Pchlide-C18 and NADPH···Pchlide-C17 interactions are shown as dotted black lines.

Thermostability Measurements and MD Simulations Corroborate Different Apo- and Holoprotein Dynamics. To assess if the observed altered protein dynamics of the apo- and holoprotein manifest itself in different thermal stabilities, we performed nano-DSF-based melting experiments and monitored the thermostability of both the apo- and the holoprotein at elevated temperatures (Figure S3). The experiments revealed grossly similar melting behavior for the apo- and holoprotein, whereby the holoprotein sample showed a slightly reduced melting temperature (T_m = 69.7 ± 0.1 °C) compared to the corresponding apoprotein sample (T_m = 70.4 ± 0.1 °C) as well as reduced thermostability (holo: $t_{1/2}$ = 67.0 ± 3.4 min; apo: $t_{1/2}$ = 95.2 ± 9.1 min). In light of the above presented neutron scattering experiments, the results are interpreted as follows: thermal stability is governed by the difference of free energy ΔG between the unfolded and folded state. The free-energy difference $\Delta G = \Delta H - T\Delta S$ consists of two parts; the first component ΔH accounts for enthalpic contributions due to internal protein forces and interactions, whereas the second term $T\Delta S$ represents the entropic component. As shown by nano-DSF, the apoprotein is found to be more thermostable than the holoprotein. This demonstrates that the enthalpic contribution due to the interactions of the protein with the bound Pchlide substrate and NADPH cofactor in the holoprotein ternary complex does not play an essential role for thermal stability. QENS experiments (see above) show that apo-LPOR is more flexible than the holoprotein. Thus, the larger flexibility of apo-LPOR results in an entropic stabilization of the apoprotein as compared to holo-LPOR. This interpretation is in agreement with the change of molecular diffusivity in the protein upon NADPH/Pchlide binding, as observed by QENS: the formation of the ternary LPOR/NADPH/Pchlid holoprotein complex does not modify the energetic barriers of molecular motions in the protein significantly. Therefore, enthalpic thermal stabilization does not occur for holo-LPOR.

MD simulations were performed to gain an atomistic understanding of the experimental neutron scattering results (Figure 3). Since so far no LPOR crystal structure is available, we employed a recent homology model of the *Te*LPOR enzyme[21] as the starting model for our simulations. This model was generated based on a previous homology model presented for the homologous LPOR of *Synechocystis* sp.[57] and was refined by a combination of homology modeling, MD simulations, hybrid quantum mechanics molecular mechanics calculations, and computational vibrational and electronic spectroscopies to yield a catalytically competent active-site geometry and reproduce characteristic experimental spectral

DOI: 10.1021/acs.jpcb.9b06608
J. Phys. Chem. B 2019, 123, 7372−7384

features.[21] Three independent 20 ns MD simulations of the NADPH/Pchlide free *Te*LPOR apoprotein and the ternary *Te*LPOR/NADPH/Pchlide holoprotein complex were performed. All simulations converged after about 5−10 ns, yielding final backbone RMSD values of ∼6 Å (apoprotein) and ∼3 Å (holoprotein) (Figure S4). As a proxy for the QENS-determined RMSD values ($\sqrt{\langle u^2 \rangle}$; Table 1), we determined the RMSD(τ) corresponding to the RMSF over all residues, of all nonexchangeable hydrogen atoms from the MD trajectories of apo- and holo-*Te*LPOR after convergence of the backbone RMSD (Figure S4, t = 10 ns) using a time window of 1 ns. This yields average values of 2.12 and 1.62 Å for the apo- and holoprotein, respectively.

Those values are slightly lower than the QENS-determined $\sqrt{\langle u^2 \rangle}$ values. Nevertheless, the same overall trend, that is, the apoprotein being more flexible than the holoprotein, is observed (Table 1). The average lower RMSD(τ) values determined from the MD simulations could hereby result from neglecting the mobility of structural elements that were not present in the homology model used for the simulations. These elements include the 20 amino acid long N-terminal His_6-tag and 30 C-terminal amino acids. To gain a better understanding of the localized dynamics of the system, we determined the average RMSF per residue at a time resolution of 1 ns for all nonexchangeable hydrogen atoms of the protein (Figure 3A). The individual data for the three independent simulations of the apo- and holoprotein is shown in Figure S5. Hereby, the apoprotein shows globally increased RMSF values compared to the holoprotein (Figure 3B). Higher RMSF values indicate greater flexibility during the MD simulation, corroborating the above presented neutron-scattering experiments, in which we observed a larger internal flexibility for the apoprotein. The most pronounced RMSF differences were observed for the N-terminal β_1−α_A loop (residues 13−17; highlighted in light orange in Figure 3A−D), which is involved in NADPH binding (GxxxGxG motif) and the C-terminal substrate binding domain (residues 235−256; highlighted in dark orange in Figure 3A−D), which coordinates the Pchlide substrate (probed e.g., in ref 58). A more detailed RMSF comparison for selected "active site" residues implicated in NADPH and Pchlide binding as well as substrate turnover is shown in Figure 3D−F. Interestingly, Y193 and K197, the two most important residues of the catalytic YxxxK motif (marked by blue horizontal bars in Figure 3A,B,D),[59] as well as most residues on the extended LPOR loop (constituted by parts of the β_5−α_E loop and α_E helix; highlighted by a light-blue line in Figure 3A,B), that distinguishes LPORs from other SDRs and in our model is part of the Pchlide binding cleft, show similar mobility in both apo- and holo-*Te*LPOR (Figure 3D−F). The conformation and mobility of these elements thus appear not to be influenced by Pchlide/NADPH binding.

Clustering of conformers sampled by MD simulations was carried out to understand the effect of Pchlide and NADPH binding on the dynamic fluctuations of the *Te*LPOR active site (34 residues listed in Figure 3D) in its apo and holo forms. In the clustering procedure, conformations are considered as different, when the RMSD for the superposition between the corresponding backbone heavy atoms was greater than 2.0 Å. As clearly seen in Figure S6, a larger number of clusters (10−24 clusters) are detected in the apoprotein simulations, whereas in all holoprotein trajectories, on average, only three to four highly populated clusters are detected. This observation is in agreement with the RMSF analysis shown in Figure S5 and corroborates the notion of much more diverse apoprotein active site dynamics, both in terms of absolute fluctuation and substrate sampling, as also detected by QENS. At the same time, this indicates that from the large ensemble of apoprotein active site conformations, a quite specific configuration is selected after Pchlide and NADPH binding.

DISCUSSION

Because of the lack of an LPOR X-ray structure, the structural and dynamic consequences of the formation of the NADPH/Pchlide/LPOR ternary holoprotein complex remain elusive, and the existence and nature of the photoactivated state in LPORs is still controversially discussed.[11,15,20] Our activity and stability measurements performed with *Te*LPOR provide unequivocal proof that preillumination of *Te*LPOR results in the formation of a photoactivated state, which in the dark decays over extended periods of time ($\tau_{act} \approx 130$ h). In light of our presented data along with the previous finding,[20] we thus redefine photoactivation as the structural/dynamic process that is triggered by limited Pchlide turnover and/or the presence of Pchlide−Chlide dimers in the protein, resulting in increased LPOR activity after low-light steady-state preillumination. Mechanistically, this could be achieved, for example, by allosteric activation of the enzyme by the Chlide reaction product, a phenomenon which has been reported for several enzymes[60−63] to contribute to the fast and coordinated transition to altered environmental conditions.[62] The magnitude of activation (11% increase in activity due to preillumination) is small but well reproducible. For other enzymatic systems, known to be allosterically activated by the product of their enzymatic reaction, similar small values have been reported. For example, for phosphoinositide phosphatases, such as the human PTEN (phosphatase and tensin homologue deleted on chromosome 10) phosphatase and the myotubularin phosphatidylinositol 3-phosphatase MTM1, allosteric product activation caused a maximal increase in activity of about 30 and 50%, respectively.[60,61]

The stability of *Te*LPOR along with the observed slow decay of the photoactivated state allowed us to study the dynamics of the apoprotein, the NADPH/Pchlide/TeLPOR holoprotein ternary complex, as well as the photoactivated holoprotein by QENS. QENS hereby provides direct information about internal flexibility and thus the sampled conformational space as well as information about internal diffusive motions interpretable in terms of the accessible energetic landscape and the rate of conformational transitions within a given conformational state. This picture assumes that the protein does not exist in one fixed configuration but instead fluctuates within and between slightly different structural states, also termed conformational substates by Frauenfelder et al.[54] Diffusive motions hereby correspond to motions within the conformational substate, whereas the residence time τ (see above, Table 1) describes the average time that the H atoms are sitting in one conformational substate. Figure 4 illustrates the structural and dynamic consequence of holoprotein formation and photoactivation, as inferred from the presented QENS experiments and MD simulations.

Our experimental QENS data clearly show different internal dynamics for the *Te*LPOR apo- and holoprotein and reveal more subtle differences for the holoprotein upon photoactivation. In the apo state, the protein is characterized by a larger internal flexibility (larger MSD value; Table 1) as

DOI: 10.1021/acs.jpcb.9b06608
J. Phys. Chem. B 2019, 123, 7372−7384

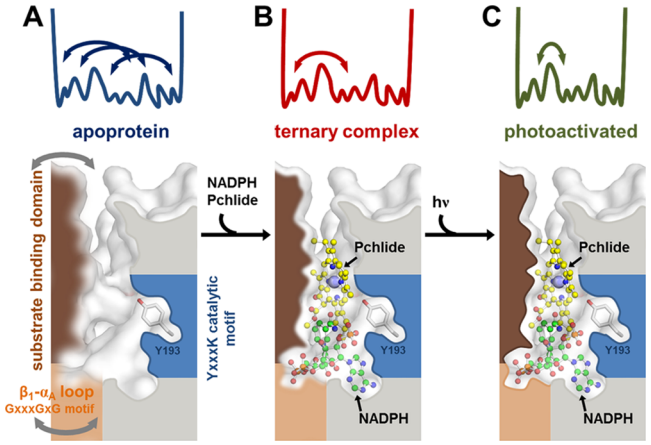

Figure 4. Dynamic and structural consequences of ternary holoprotein complex formation and photoactivation. Schematic illustration of sampled energetic landscape of *Te*LPOR and the structure of the *Te*LPOR NADPH and Pchlide binding site within the apoprotein (A), the NADPH/Pchlide/*Te*LPOR ternary holoprotein complex (B), and the photoactivated holoprotein (C). Structural regions involved in NADPH and Pchlide binding, such as the substrate binding domain (dark orange), the $\beta_1-\alpha_A$ loop GxxxGxG motif (light orange), and the YxxxK catalytic motif (blue), are highlighted. Flexibility of the respective region is indicated by blurred-drawn regions. The catalytic tyrosine (Y193) of *Te*LPOR is shown in stick representation.

compared to the dark-adapted holoprotein. On the other hand, the observed internal diffusivity in the apoprotein is reduced, and the residence time between local jumps is increased in comparison to the dark-adapted holoprotein complex (Table 1). Internal diffusion coefficients and residence times are informative on energetic barriers between slightly different structural substates and rates of conformational transitions of the protein, whereas the MSD is a measure of the conformational space that is accessible to the protein (Figure 4A; top). The larger MSD value of the apoprotein demonstrates a larger conformational space that is sampled by the ligand free apoprotein. The slower internal diffusion coefficient and the larger residence time of the apoprotein, however, both indicate that transitions between conformational substates that are separated by relatively large energetic barriers are accessible for the apoprotein. This would enable the protein to sample multiple conformations in its apoprotein form, which might contribute to the binding of the bulky Pchlide substrate and the NADPH cofactor. This is also corroborated by the above presented clustering analysis performed in the MD trajectories of the apo- and holoprotein (Figure S6). Previously, both Pchlide and NADPH binding to *Te*LPOR were shown to be a complex process involving multiple conformational changes in the protein to yield the active ternary enzyme–substrate complex "poised" for catalysis,[64] thus corroborating the here-presented dynamic analysis. In terms of structure, as judged from our MD simulations, the majority of flexibility observed for the apoprotein stems from structural fluctuations of the NADPH and Pchlide binding sites (substrate binding domain and $\beta_1-\alpha_A$ loop GxxxGxG motif; Figures 3C and 4A; marked in dark and light orange) of *Te*LPOR. Interestingly, for *E. coli* DHFR, it was shown that the dynamics of the region corresponding to the $\beta_1-\alpha_A$ loop (called Met20-loop in DHFR) are directly linked to enzyme catalysis as mutations that abrogated millisecond fluctuations of the loop impaired hydride transfer.[65] In contrast, the structural region harboring the catalytic YxxxK motif as well as the remainder of the structure (Figures 3C and 4A; marked in blue) remains relatively rigid.

Pchlide/NADPH binding in the dark-adapted holoprotein results in a stiffer protein conformation with a reduced MSD value demonstrating a restricted conformational space (Figure 4B). At the same time, we observe a faster internal diffusion coefficient and a decreased residence time as compared to apo-*Te*LPOR (Table 1). In the molecular picture, NADPH/Pchlide binding appears not to modify the energetic barriers between conformational substates significantly, which is corroborated by our thermal stability measurements (see Results section and Figure S3). Instead, it seems to restrict the amplitudes of motions due to structural constraints. As a consequence, only local transitions between conformational substates are possible that are not separated by large energetic barriers, which effectively results in an increase of the internal diffusion coefficient and a reduction of the residence time. A similar observation has been made recently for the internal ns dynamics of folded and unfolded bovine serum albumin (BSA)[51] and retinal bound and free rhodopsin.[66] Amplitudes of motion in folded BSA are reduced as compared to the unfolded state, but internal molecular diffusivity in folded BSA is significantly faster than in the unfolded state. Concerning rhodopsin, faster motions have been found for the holoprotein complex, whereas slower motions have been observed for the apoprotein being in agreement with the observed change of internal diffusivity for holo- and apo-*Te*LPOR reported in this study.

Photoactivation of the holoprotein has a more subtle effect on internal protein dynamics. Molecular motions in the photoactivated *Te*LPOR complex are reduced in amplitude as compared to the dark-adapted holoprotein (Figure 4C). At the same time, the internal diffusion coefficient of photoactivated *Te*LPOR is reduced, whereas residence times remain on a comparative level. Together with the lower MSD value of photoactivated *Te*LPOR, a different dynamic mechanism might need to be considered here as an explanation: photoactivation of *Te*LPOR restricts the accessible conformational space of the active protein, and at the same time internal motions are slowed down, which is visible by the reduced internal diffusion coefficients. Hence, we interpret the different dynamic behavior of the photoactivated holoprotein as a stiffer conformation compared to the dark-adapted holoprotein, which in a structural sense could be interpreted as further rigidification of the NADPH/Pchlide binding site of *Te*LPOR (Figure 4C). This rigidification, resulting in optimized active site geometries, could then be the cause for increased Pchlide turnover after preillumination, that is, due to the presence of Pchlide–Chlide dimers in the protein[20] (see above). In previous studies on the thermal adaptation of extremophilic bacteria and enzymes, it has been observed that protein dynamics need to be maintained in a certain limit with a $\sqrt{\langle u^2 \rangle}$ values between 1.2 and 1.5 Å on the 0.1 ns time scale[67,68] to enable optimal growth of bacteria and to achieve maximal catalytic activity of enzymes. Neutron spectroscopy studies investigating the adaptation of hemoglobin to species' body temperature confirmed that observation and reported hemoglobin fluctuations on the 0.1 ns time sale with a $\sqrt{\langle u^2 \rangle}$ value between 1.2 and 1.4 Å at the species' body

DOI: 10.1021/acs.jpcb.9b06608
J. Phys. Chem. B 2019, 123, 7372–7384

temperature.[69] The observed reduction of the dynamics of LPOR due to photoactivation is reminiscent of those studies. The $\sqrt{\langle u^2 \rangle}$ value of photoactivated *Te*LPOR is slightly larger than those optimal values reported on the 0.1 ns time scale, as the SPHERES neutron spectrometer is sensitive to slower motions taking place up to a few ns. It therefore appears that the LPOR dynamics need to be reduced in amplitude to allow for optimal enzymatic function in the photoactivated state. Such a process would be even more important at elevated temperatures, that is, under which the thermophilic cyanobacterium *T. elongatus* optimally grows,[70] because at higher temperatures, active site rigidity would become compromised by the overall increase in thermal fluctuations.

CONCLUSIONS

We here analyzed the internal protein dynamics of a LPOR in its NADPH/Pchlide free apo form, the dark-adapted reconstituted LPOR/NADPH/Pchlide holoprotein ternary complex, and the ternary complex after photoactivation, with the latter process being redefined here as the structural/dynamic process that is triggered by limited Pchlide turnover due to low-light steady-state preillumination. Our studies provide compelling evidence that photoactivation increases the rate of catalysis, which in light of the here-presented data and previous findings[15] is likely linked to the formation of Pchlide−Chlide dimers in the protein. Low-level light, leading to LPOR photoactivation, would hereby provide an adaptive cue "readying" the enzyme for catalysis, thereby enabling the use of low or erratic photon fluxes. QENS experiments, to the best of our knowledge, applied for the first time here to a photoenzyme, revealed different internal protein dynamics for the apo-LPOR protein, the dark-adapted ternary holoprotein complex, and the photoactivated holoprotein. The formation of the ternary holoprotein complex as well as photoactivation results in progressive rigidification of the protein. Photoactivation of the ternary protein−ligand complex results in reduced dynamics that are essential for increased enzyme activity, which could become even more important at elevated temperatures under which *T. elongatus*, the thermophilic cyanobacterium that harbors *Te*LPOR, dwells. On the basis of MD simulations, the majority of the flexibility observed for the apoprotein stems from structural fluctuations of the NADPH and Pchlide binding sites of *Te*LPOR, with the rigidification of the dark-adapted and the photoactivated holoprotein, therefore, likely occurring at those sites. Importantly, our findings stress the importance of the intricate balance between protein flexibility and rigidity for enzyme−substrate complex formation and optimal catalysis, thereby providing a link between protein dynamics and catalytic function.

ASSOCIATED CONTENT

Supporting Information

The Supporting Information is available free of charge on the ACS Publications website at DOI: 10.1021/acs.jpcb.9b06608.

Adaptation of the steady-state illumination conditions, decay of the photoactivated state of *Te*LPOR, melting and thermostability measurements for the *Te*LPOR apo- and holoprotein, time evolution of the backbone RMSD of three independent MD simulations of apo- and holo-*Te*LPOR, RMSF per residue for three independent MD simulations of apo- and holo-*Te*LPOR, and clustering of sampled structures during MD simulations of apo- and holo-*Te*LPOR (PDF)

AUTHOR INFORMATION

Corresponding Authors

*E-mail: a.stadler@fz-juelich.de. Phone: +49 2461-61-4502 (A.M.S.).

*E-mail: u.krauss@fz-juelich.de. Phone: +49 2461-61-2939 (U.K.).

ORCID

Andreas Maximilian Stadler: 0000-0003-2272-5232

Samira Gholami: 0000-0002-8133-0890

Ulrich Schwaneberg: 0000-0003-4026-701X

Ivan Rivalta: 0000-0002-1208-602X

Marco Garavelli: 0000-0002-0796-289X

Mehdi D. Davari: 0000-0003-0089-7156

Karl-Erich Jaeger: 0000-0002-6036-0708

Ulrich Krauss: 0000-0003-2219-7388

Present Address

♦Department of Chemistry, Bowling Green State University, Bowling Green, Ohio 43403, United States.

Author Contributions

U.K. and A.S. conceived the study. U.K., A.M.S., J.S., and E.K.-G. planned the experiments. J.S. generated constructs, purified the protein, and prepared QENS samples with the help of E.K.-G. J.S. carried out all UV−vis spectrophotometric analyses, activity, and nano-DSF measurements. A.M.S. and M.Z. performed QENS experiments and analyzed the corresponding data. S.G., I.R., M.G., and M.D.D. performed and analyzed MD simulations. U.K., J.S., and A.M.S. analyzed and interpreted the data. U.K., J.S., and A.M.S. wrote the manuscript with contributions from all authors. All authors discussed the results and commented on the manuscript.

Notes

The authors declare no competing financial interest.

ACKNOWLEDGMENTS

This work is based upon experiments performed on the instrument SPHERES operated by the Jülich Centre for Neutron Science at the Heinz Maier-Leibnitz Zentrum, Garching. J.S. and U.K. acknowledge funding by the Deutsche Forschungsgemeinschaft (DFG) (Grant "Origin, phylogeny, evolution and structural basis of light-driven Pchlide reduction"; KR 3756/1-1). Simulations were partially performed with computing resources granted by JARA-HPC from the RWTH Aachen University under project JARA0065.

REFERENCES

(1) Zhang, H.; Kenaan, C.; Hamdane, D.; Hoa, G. H. B.; Hollenberg, P. F. Effect of Conformational Dynamics on Substrate Recognition and Specificity as Probed by the Introduction of a de Novo Disulfide Bond into Cytochrome P450 2B1. *J. Biol. Chem.* **2009**, *284*, 25678−25686.

(2) Epstein, D. M.; Benkovic, S. J.; Wright, P. E. Dynamics of the dihydrofolate reductase-folate complex: catalytic sites and regions known to undergo conformational change exhibit diverse dynamical features. *Biochemistry* **1995**, *34*, 11037−11048.

(3) Vaughn, M. B.; Zhang, J.; Spiro, T. G.; Dyer, R. B.; Klinman, J. P. Activity-Related Microsecond Dynamics Revealed by Temperature-Jump Förster Resonance Energy Transfer Measurements on Thermophilic Alcohol Dehydrogenase. *J. Am. Chem. Soc.* **2018**, *140*, 900−903.

DOI: 10.1021/acs.jpcb.9b06608
J. Phys. Chem. B 2019, 123, 7372−7384

(4) Wong, K. F.; Selzer, T.; Benkovic, S. J.; Hammes-Schiffer, S. Impact of distal mutations on the network of coupled motions correlated to hydride transfer in dihydrofolate reductase. *Proc. Natl. Acad. Sci. U.S.A.* **2005**, *102*, 6807−6812.
(5) Wolf-Watz, M.; Thai, V.; Henzler-Wildman, K.; Hadjipavlou, G.; Eisenmesser, E. Z.; Kern, D. Linkage between dynamics and catalysis in a thermophilic-mesophilic enzyme pair. *Nat. Struct. Mol. Biol.* **2004**, *11*, 945−949.
(6) Kohen, A. Dihydrofolate reductase as a model for studies of enzyme dynamics and catalysis. *F1000Res* **2015**, *4*, 1464.
(7) Luk, L. Y. P.; Javier Ruiz-Pernia, J.; Dawson, W. M.; Roca, M.; Loveridge, E. J.; Glowacki, D. R.; Harvey, J. N.; Mulholland, A. J.; Tunon, I.; Moliner, V.; et al. Unraveling the role of protein dynamics in dihydrofolate reductase catalysis. *Proc. Natl. Acad. Sci. U.S.A.* **2013**, *110*, 16344−16349.
(8) Singh, P.; Abeysinghe, T.; Kohen, A. Linking protein motion to enzyme catalysis. *Molecules* **2015**, *20*, 1192−1209.
(9) Singh, P.; Francis, K.; Kohen, A. Network of remote and local protein dynamics in dihydrofolate reductase catalysis. *ACS Catal.* **2015**, *5*, 3067−3073.
(10) Kaschner, M.; Loeschcke, A.; Krause, J.; Minh, B. Q.; Heck, A.; Endres, S.; Svensson, V.; Wirtz, A.; von Haeseler, A.; Jaeger, K.-E.; et al. Discovery of the first light-dependent protochlorophyllide oxidoreductase in anoxygenic phototrophic bacteria. *Mol. Microbiol.* **2014**, *93*, 1066−1078.
(11) Björn, L. O. Photoenzymes and related topics: an update. *Photochem. Photobiol.* **2018**, *94*, 459−465.
(12) Gabruk, M.; Mysliwa-Kurdziel, B. Light-dependent protochlorophyllide oxidoreductase: phylogeny, regulation, and catalytic properties. *Biochemistry* **2015**, *54*, 5255−5262.
(13) Reinbothe, C.; Bakkouri, M. E.; Buhr, F.; Muraki, N.; Nomata, J.; Kurisu, G.; Fujita, Y.; Reinbothe, S. Chlorophyll biosynthesis: spotlight on protochlorophyllide reduction. *Trends Plant Sci.* **2010**, *15*, 614−624.
(14) Heyes, D. J.; Ruban, A. V.; Wilks, H. M.; Hunter, C. N. Enzymology below 200 K: the kinetics and thermodynamics of the photochemistry catalyzed by protochlorophyllide oxidoreductase. *Proc. Natl. Acad. Sci. U.S.A.* **2002**, *99*, 11145−11150.
(15) Sytina, O. A.; Heyes, D. J.; Hunter, C. N.; Alexandre, M. T.; van Stokkum, I. H. M.; van Grondelle, R.; Groot, M. L. Conformational changes in an ultrafast light-driven enzyme determine catalytic activity. *Nature* **2008**, *456*, 1001−1004.
(16) Heyes, D. J.; Hardman, S. J. O.; Hedison, T. M.; Hoeven, R.; Greetham, G. M.; Towrie, M.; Scrutton, N. S. Excited-state charge separation in the photochemical mechanism of the light-driven enzyme protochlorophyllide oxidoreductase. *Angew. Chem., Int. Ed. Engl.* **2015**, *54*, 1512−1515.
(17) Sytina, O. A.; van Stokkum, I. H. M.; Heyes, D. J.; Hunter, C. N.; Groot, M. L. Spectroscopic characterization of the first ultrafast catalytic intermediate in protochlorophyllide oxidoreductase. *Phys. Chem. Chem. Phys.* **2012**, *14*, 616−625.
(18) Archipowa, N.; Kutta, R. J.; Heyes, D. J.; Scrutton, N. S. Stepwise hydride transfer in a biological system: insights into the reaction mechanism of the light-dependent protochlorophyllide oxidoreductase. *Angew. Chem., Int. Ed. Engl.* **2018**, *57*, 2682−2686.
(19) Sytina, O. A.; Alexandre, M. T.; Heyes, D. J.; Hunter, C. N.; Robert, B.; van Grondelle, R.; Groot, M. L. Enzyme activation and catalysis: characterisation of the vibrational modes of substrate and product in protochlorophyllide oxidoreductase. *Phys. Chem. Chem. Phys.* **2011**, *13*, 2307−2313.
(20) Heyes, D. J.; Hardman, S. J. O.; Mansell, D.; Gardiner, J. M.; Scrutton, N. S. Mechanistic reappraisal of early stage photochemistry in the light-driven enzyme protochlorophyllide oxidoreductase. *PLoS One* **2012**, *7*, No. e45642.
(21) Gholami, S.; Nenov, A.; Rivalta, I.; Bocola, M.; Bordbar, A. K.; Schwaneberg, U.; Davari, M. D.; Garavelli, M. Theoretical model of the protochlorophyllide oxidoreductase from a hierarchy of protocols. *J. Phys. Chem. B* **2018**, *122*, 7668−7681.
(22) Heyes, D. J.; Scrutton, N. S. Conformational changes in the catalytic cycle of protochlorophyllide oxidoreductase: what lessons can be learnt from dihydrofolate reductase? *Biochem. Soc. T.* **2009**, *37*, 354−357.
(23) Lechner, R. E.; Longeville, S. Quasielastic Neutron Scattering in Biology, Part II: Applications. In *Neutron Scattering in Biology-Techniques and Applications*; Fitter, J., Gutberlet, T., Katsaras, J., Eds.; Springer-Verlag: Berlin Heidelberg, 2006.
(24) Studier, F. W. Protein production by auto-induction in high-density shaking cultures. *Protein Expr. Purif.* **2005**, *41*, 207−234.
(25) Heyes, D. J.; Hunter, C. N. Identification and Characterization of the Product Release Steps within the Catalytic Cycle of Protochlorophyllide Oxidoreductase. *Biochemistry* **2004**, *43*, 8265−8271.
(26) Heyes, D. J.; Martin, G. E. M.; Reid, R. J.; Hunter, C. N.; Wilks, H. M. NADPH:protochlorophyllide oxidoreductase from *Synechocystis* : overexpression, purification and preliminary characterisation. *FEBS Lett.* **2000**, *483*, 47−51.
(27) Yang, Z. M.; Bauer, C. E. *Rhodobacter capsulatus* genes involved in early steps of the bacteriochlorophyll biosynthetic pathway. *J. Bacteriol.* **1990**, *172*, 5001−5010.
(28) Wuttke, J.; Budwig, A.; Drochner, M.; Kämmerling, H.; Kayser, F.-J.; Kleines, H.; Ossovyi, V.; Pardo, L. C.; Prager, M.; Richter, D.; et al. SPHERES, Jülich's high-flux neutron backscattering spectrometer at FRM II. *Rev. Sci. Instrum.* **2012**, *83*, 075109.
(29) Zamponi, M.; Khaneft, M. SPHERES: Backscattering spectrometer. *J. Large Scale Res. Fac.* **2015**, *1*, A30.
(30) Bée, M. *Quasielastic Neutron Scattering: Principles and Applications in Solid State Chemistry, Biology, and Materials Science*; Adam Hilger: Bristol, England, 1988, DOI: 10.17815/jlsrf-1-38.
(31) Pérez, J.; Zanotti, J.-M.; Durand, D. Evolution of the internal dynamics of two globular proteins from dry powder to solution. *Biophys. J.* **1999**, *77*, 454−469.
(32) Roosen-Runge, F.; Hennig, M.; Zhang, F.; Jacobs, R. M. J.; Sztucki, M.; Schober, H.; Seydel, T.; Schreiber, F. Protein self-diffusion in crowded solutions. *Proc. Natl. Acad. Sci. U.S.A.* **2011**, *108*, 11815−11820.
(33) Stadler, A. M.; van Eijck, L.; Demmel, F.; Artmann, G. Macromolecular dynamics in red blood cells investigated using neutron spectroscopy. *J. R. Soc. Interface* **2011**, *8*, 590−600.
(34) Olsson, M. H. M.; Søndergaard, C. R.; Rostkowski, M.; Jensen, J. H. PROPKA3: consistent treatment of internal and surface residues in empirical pKa predictions. *J. Chem. Theory Comput.* **2011**, *7*, 525−537.
(35) Case, D. A.; Darden, T. A.; Cheatham, I.; Simmerling, C. L.; Wang, J.; Duke, R. E.; Luo, R.; Walker, R. C.; Zhang, W.; Merz, K. M.; et al. *AMBER 12*; University of California: San Francisco, 2012.
(36) Li, D.-W.; Brüschweiler, R. NMR-Based Protein Potentials. *Angew. Chem., Int. Ed. Engl.* **2010**, *122*, 6930−6932.
(37) Lindorff-Larsen, K.; Piana, S.; Palmo, K.; Maragakis, P.; Klepeis, J. L.; Dror, R. O.; Shaw, D. E. Improved side-chain torsion potentials for the Amber ff99SB protein force field. *Proteins: Struct. Funct. Bioinf.* **2010**, *78*, 1950−1958.
(38) Jorgensen, W. L.; Chandrasekhar, J.; Madura, J. D.; Impey, R. W.; Klein, M. L. Comparison of simple potential functions for simulating liquid water. *J. Chem. Phys.* **1983**, *79*, 926−935.
(39) Essmann, U.; Perera, L.; Berkowitz, M. L.; Darden, T.; Lee, H.; Pedersen, L. G. A smooth particle mesh Ewald method. *J. Chem. Phys.* **1995**, *103*, 8577−8593.
(40) Berendsen, H. J. C.; Postma, J. P. M.; van Gunsteren, W. F.; DiNola, A.; Haak, J. R. Molecular dynamics with coupling to an external bath. *J. Chem. Phys.* **1984**, *81*, 3684−3690.
(41) Case, D. A.; Babin, V.; Berryman, J.; Betz, R. M.; Cai, Q.; Cerutti, D. S.; Cheatham, I.; Darden, T. A.; Duke, R. E.; Gohlke, H.; et al. *AMBER 14*; University of California: San Francisco, 2014.
(42) Schrödinger, L. *The PyMOL molecular graphics system*, version 1.3 r1, 2010.
(43) Stadler, A. M.; Pellegrini, E.; Johnson, M.; Fitter, J.; Zaccai, G. Dynamics-stability relationships in apo- and holomyoglobin: a

DOI: 10.1021/acs.jpcb.9b06608
J. Phys. Chem. B 2019, 123, 7372−7384

combined neutron scattering and molecular dynamics simulations study. *Biophys. J.* **2012**, *102*, 351−359.
(44) Feig, M.; Karanicolas, J.; Brooks, C. L., 3rd MMTSB Tool Set: enhanced sampling and multiscale modeling methods for applications in structural biology. *J. Mol. Graph. Model.* **2004**, *22*, 377−395.
(45) McFarlane, M. J.; Hunter, C. N.; Heyes, D. J. Kinetic characterisation of the light-driven protochlorophyllide oxidoreductase (POR) from *Thermosynechococcus elongatus*. *Photochem. Photobiol. Sci.* **2005**, *4*, 1055−1059.
(46) Chahdi, M. A. O.; Schoefs, B.; Franck, F. Isolation and characterization of photoactive complexes of NADPH : protochlorophyllide oxidoreductase from wheat. *Planta* **1998**, *206*, 673−680.
(47) Martin, G. E. M.; Timko, M. P.; Wilks, H. M. Purification and kinetic analysis of pea (*Pisum sativum* L.) NADPH:protochlorophyllide oxidoreductase expressed as a fusion with maltose-binding protein in *Escherichia coli*. *Biochem. J.* **1997**, *325*, 139−145.
(48) Townley, H. E.; Griffiths, W. T.; Nugent, J. P. A reappraisal of the mechanism of the photoenzyme protochlorophyllide reductase based on studies with the heterologously expressed protein. *FEBS Lett.* **1998**, *422*, 19−22.
(49) Lebedev, N.; Timko, M. P. Protochlorophyllide oxidoreductase B-catalyzed protochlorophyllide photoreduction *in vitro*: insight into the mechanism of chlorophyll formation in light-adapted plants. *Proc. Natl. Acad. Sci. U.S.A.* **1999**, *96*, 9954−9959.
(50) Stadler, A. M.; Digel, I.; Artmann, G. M.; Embs, J. P.; Zaccai, G.; Büldt, G. Hemoglobin dynamics in red blood cells: correlation to body temperature. *Biophys. J.* **2008**, *95*, 5449−5461.
(51) Ameseder, F.; Radulescu, A.; Khaneft, M.; Lohstroh, W.; Stadler, A. M. Homogeneous and heterogeneous dynamics in native and denatured bovine serum albumin. *Phys. Chem. Chem. Phys.* **2018**, *20*, 5128−5139.
(52) Biehl, R.; Hoffmann, B.; Monkenbusch, M.; Falus, P.; Preost, S.; Merkel, R.; Richter, D. Direct observation of correlated interdomain motion in alcohol dehydrogenase. *Phys. Rev. Lett.* **2008**, *101*, 138102.
(53) Monkenbusch, M.; Stadler, A.; Biehl, R.; Ollivier, J.; Zamponi, M.; Richter, D. Fast internal dynamics in alcohol dehydrogenase. *J. Chem. Phys.* **2015**, *143*, 075101.
(54) Frauenfelder, H.; Parak, F.; Young, R. D. Conformational substates in proteins. *Annu. Rev. Biophys. Biophys. Chem.* **1988**, *17*, 451−479.
(55) Bicout, D. J.; Zaccai, G. Protein Flexibility from the Dynamical Transition:A Force Constant Analysis. *Biophys. J.* **2001**, *80*, 1115−1123.
(56) Zaccai, G. How Soft Is a Protein? A Protein Dynamics Force Constant Measured by Neutron Scattering. *Science* **2000**, *288*, 1604−1607.
(57) Townley, H. E.; Sessions, R. B.; Clarke, A. R.; Dafforn, T. R.; Griffiths, W. T. Protochlorophyllide oxidoreductase: a homology model examined by site-directed mutagenesis. *Proteins* **2001**, *44*, 329−335.
(58) Menon, B. R. K.; Hardman, S. J. O.; Scrutton, N. S.; Heyes, D. J. Multiple active site residues are important for photochemical efficiency in the light-activated enzyme protochlorophyllide oxidoreductase (POR). *J. Photochem. Photobiol. B.* **2016**, *161*, 236−243.
(59) Wilks, H. M.; Timko, M. P. A light-dependent complementation system for analysis of NADPH:protochlorophyllide oxidoreductase: identification and mutagenesis of two conserved residues that are essential for enzyme activity. *Proc. Natl. Acad. Sci. U.S.A.* **1995**, *92*, 724−728.
(60) Campbell, R. B.; Liu, F.; Ross, A. H. Allosteric activation of PTEN phosphatase by phosphatidylinositol 4,5-bisphosphate. *J. Biol. Chem.* **2003**, *278*, 33617−33620.
(61) Schaletzky, J.; Dove, S. K.; Short, B.; Lorenzo, O.; Clague, M. J.; Barr, F. A. Phosphatidylinositol-5-phosphate activation and conserved substrate specificity of the myotubularin phosphatidylinositol 3-phosphatases. *Curr. Biol.* **2003**, *13*, 504−509.
(62) Shyp, V.; Tankov, S.; Ermakov, A.; Kudrin, P.; English, B. P.; Ehrenberg, M.; Tenson, T.; Elf, J.; Hauryliuk, V. Positive allosteric feedback regulation of the stringent response enzyme RelA by its product. *EMBO Rep.* **2012**, *13*, 835−839.
(63) Zhong, S.; Hsu, F.; Stefan, C. J.; Wu, X.; Patel, A.; Cosgrove, M. S.; Mao, Y. Allosteric activation of the phosphoinositide phosphatase Sac1 by anionic phospholipids. *Biochemistry* **2012**, *51*, 3170−3177.
(64) Heyes, D. J.; Menon, B. R. K.; Sakuma, M.; Scrutton, N. S. Conformational Events during Ternary Enzyme−Substrate Complex Formation Are Rate Limiting in the Catalytic Cycle of the Light-Driven Enzyme Protochlorophyllide Oxidoreductase. *Biochemistry* **2008**, *47*, 10991−10998.
(65) Bhabha, G.; Lee, J.; Ekiert, D. C.; Gam, J.; Wilson, I. A.; Dyson, H. J.; Benkovic, S. J.; Wright, P. E. A dynamic knockout reveals that conformational fluctuations influence the chemical step of enzyme catalysis. *Science* **2011**, *332*, 234−238.
(66) Shrestha, U. R.; Perera, S. M. D. C.; Bhowmik, D.; Chawla, U.; Mamontov, E.; Brown, M. F.; Chu, X.-Q. Quasi-elastic neutron scattering reveals ligand-induced protein dynamics of a G-protein-coupled receptor. *J. Phys. Chem. Lett.* **2016**, *7*, 4130−4136.
(67) Tehei, M.; Franzetti, B.; Madern, D.; Ginzburg, M.; Ginzburg, B. Z.; Giudici-Orticoni, M.-T.; Bruschi, M.; Zaccai, G. Adaptation to extreme environments: macromolecular dynamics in bacteria compared *in vivo* by neutron scattering. *EMBO Rep.* **2004**, *5*, 66−70.
(68) Tehei, M.; Madern, D.; Franzetti, B.; Zaccai, G. Neutron scattering reveals the dynamic basis of protein adaptation to extreme temperature. *J. Biol. Chem.* **2005**, *280*, 40974−40979.
(69) Stadler, A. M.; Garvey, C. J.; Bocahut, A.; Sacquin-Mora, S.; Digel, I.; Schneider, G. J.; Natali, F.; Artmann, G. M.; Zaccai, G. Thermal fluctuations of haemoglobin from different species: adaptation to temperature via conformational dynamics. *J. R. Soc. Interface* **2012**, *9*, 2845−2855.
(70) Yamaoka, T.; Satoh, K.; Katoh, S. Photosynthetic activities of a thermophilic blue-green alga. *Plant Cell Physiol.* **1978**, *19*, 943−954.

DOI: 10.1021/acs.jpcb.9b06608
J. Phys. Chem. B 2019, 123, 7372−7384